SCIENCE CHINA
Information Sciences

• RESEARCH PAPER •

August 2025, Vol. 68, Iss. 8, 180505:1–180505:7
https://doi.org/10.1007/s11432-025-4508-4

Special Topic: Quantum Information

Bridging quantum elementary links with spectral steering

Ruiming ZHANG[1,2,3], Yunru FAN[1,2,3*], Chenzhi YUAN[1,4], Hao YU[1,2,3], Hao LI[5], You WANG[1,6], Guangwei DENG[1,3,7], Haizhi SONG[1,6*], Lixing YOU[5], Guangcan GUO[1,2,3,7] & Qiang ZHOU[1,2,3,7*]

[1]*Institute of Fundamental and Frontier Sciences, University of Electronic Science and Technology of China, Chengdu 611731, China*
[2]*Center for Quantum Internet, Tianfu Jiangxi Laboratory, Chengdu 641419, China*
[3]*Key Laboratory of Quantum Physics and Photonic Quantum Information, Ministry of Education, University of Electronic Science and Technology of China, Chengdu 611731, China*
[4]*Hubei Key Laboratory of Optical Information and Pattern Recognition, Wuhan Institute of Technology, Wuhan 430205, China*
[5]*National Key Laboratory of Materials for Integrated Circuits, Shanghai Institute of Microsystem and Information Technology, Chinese Academy of Sciences, Shanghai 200050, China*
[6]*Southwest Institute of Technical Physics, Chengdu 610041, China*
[7]*CAS Key Laboratory of Quantum Information, University of Science and Technology of China, Hefei 230026, China*

Received 8 April 2025/Revised 4 June 2025/Accepted 26 June 2025/Published online 8 July 2025

Abstract Spectrally multiplexed quantum elementary link is an important building block for quantum networks. Towards long distance quantum communication, such multiplexed elementary links should be connected via the Bell state measurement (BSM). In this work, we propose and demonstrate a scheme for connecting two adjacent elementary links with frequency shifting. In our proof-of-principle demonstration, each elementary link has two spectral channels with a channel spacing of 16 GHz, and the photonic quantum information is encoded in the temporal mode. A projection fidelity of BSM reaches >95% between different spectral channels with decoy-state analysis. We also evaluate the performance of our demonstration by calculating the secret key rate of spectrally multiplexed measurement-device-independent quantum key distribution. Our results could pave the way for developing long distance quantum networks.

Keywords spectrally multiplexing, Bell state measurement, frequency shifting, quantum elementary link, quantum network

Citation Zhang R M, Fan Y R, Yuan C Z, et al. Bridging quantum elementary links with spectral steering. Sci China Inf Sci, 2025, 68(8): 180505, https://doi.org/10.1007/s11432-025-4508-4

1 Introduction

Towards a scalable quantum network, the rate of photonic quantum entanglement distribution is inherently limited by the optical loss of the channel [1–3]. Quantum repeater provides a promising solution, which plays a pivotal role in developing scalable quantum network [4–10]. With the quantum repeater, long-distance quantum entanglement distribution can be divided into several elementary links, which are then connected by quantum entanglement swapping via the BSM [11, 12]. In parallel with developing quantum repeaters, the rate of such distribution can be further improved by multiplexing [13, 14] in different degrees of freedom of photons, such as in spectral [15–17], temporal [18, 19], and spatial [20, 21] domains. Among these methods, multiplexing in the spectral domain attracts great interest for its promising scalability as well as fixed losses and the requirement of resources [22,23]. However, the demonstration of connecting two adjacent elementary links with spectral multiplexing via the BSM remains challenging [24], due to the intrinsic distinguishability of photonic qubits from different spectral channels [6]. To achieve perfect entanglement swapping between spectral multiplexing elementary links, frequency shifting for photonic qubits is required.

* Corresponding author (email: yunrufan@uestc.edu.cn, hzsong@uestc.edu.cn, zhouqiang@uestc.edu.cn)

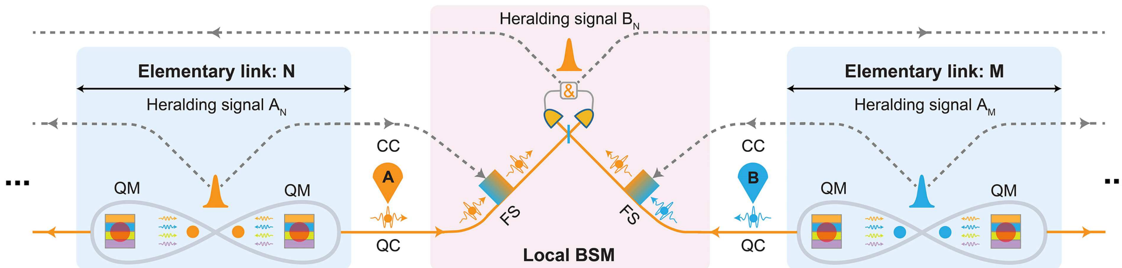

Figure 1 (Color online) Conceptual illustration of connecting two adjacent elementary links using spectral multiplexed BSM. In each elementary link N/M, the entanglement swapped photons are respectively stored in the quantum memories (QMs) located at the ends of elementary links, with spectral modes depicted in different colors. The heralding signals $\mathrm{A}_{N/M}$ generated by the successful entanglement swapping in each elementary link are sent over a classical channel (CC) to the local BSM station. Simultaneously, photons A and B are recalled from the adjacent elementary links, and transmitted to the local BSM station via quantum channels (QCs). The heralding signals $\mathrm{A}_{N/M}$ then trigger the frequency shifters (FSs) to map photons onto the desired spectral mode. Conditioned on a successful measurement in the local BSM, elementary links N and M are connected, generating the herald signal B_N for the next stage of link connection.

Here, we design and realize frequency shifting of photonic time-bin qubits within a temporal aperture defined by the ramp voltage signal on an electro-optical phase modulator, and the time-bin qubits are prepared with a weak coherent state. We further perform a proof-of-principle demonstration of the connection between two adjacent spectrally multiplexed elementary links. In our experiment, two individual spectral channels with a channel separation of 16 GHz are mapped onto a common spectral channel with the frequency shifting of the single-photon wavepacket. After erasing the distinguishability of photonic qubits in the spectral domain, we achieve the BSM with fidelities exceeding >95% between different spectral channels with decoy-state analysis. The performance of the system is also analyzed by calculating the secret key rate of a spectrally multiplexed measurement-device-independent quantum key distribution (MDI-QKD). Our result establishes an important foundation for the development of long-distance spectrally multiplexed quantum networks.

2 Experimental demonstration and results

A conceptual scheme for connecting adjacent spectrally multiplexed elementary links with frequency shifting is shown in Figure 1. In this scheme, both the Nth and the Mth elementary links, where $M = N+1$, have two spectrally multiplexed quantum memories (QMs) entangled via spectrally resolving entanglement swapping at the middle point of each link [24, 25]. Spectrally multiplexed photonic qubits A/B are stored in different spectral channels of the QMs. When the entanglement between two spectrally multiplexed QMs in the Nth elementary link is successfully established, a heralding signal, labeled as A_N, is generated. Suppose that the same process happens in the Mth elementary link with the corresponding heralded signal A_M generated. The qubit A and qubit B, respectively from the Nth and Mth elementary links, are then recalled and transmitted over their own quantum channels (QCs) to a local BSM station for entanglement swapping. The heralding signals A_N and A_M, which contain the information of the spectral modes for qubit A and qubit B, then trigger the frequency shifters (FSs) to respectively map their corresponding qubits onto the previously agreed-upon spectral channel. Once the BSM is successful and the entanglement between the two adjacent elementary links is established, the local BSM station generates a heralding signal B_N, which is then used for the next stage BSM and entanglement swapping. By repeating the procedure with other links, entanglement can be established between two distant nodes across the entire quantum channel.

To demonstrate the feasibility of frequency shifting in the local BSM station, we experimentally characterize the performance of the frequency shifter using the time-bin encoded single-photon qubits and demonstrate the BSM between different spectral channels. The schematic of our experimental setup is shown in Figure 2. The node A/B is employed to simulate the recalled photons from adjacent QMs. In order to simulate the different spectral modes for each node, we used an attenuated dual-pulse laser to prepare the time-bin qubits ($|\psi\rangle_{\mathrm{A/B}}$) with different frequency settings (see the lower left inset of Figure 2 marked "Node A/B"). The qubit ($|\psi\rangle_{\mathrm{B}}$) from node B passes through an FS to eliminate the frequency distinguishability. The FS is based on a phase modulator (PM) (see the lower right inset of Figure 2 marked "FS") and allows the single-photon frequency shifting with the magnitude from −40 to 20 GHz

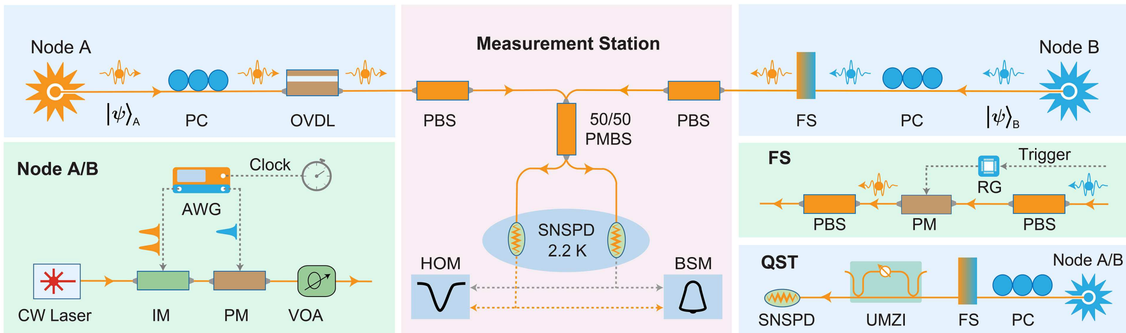

Figure 2 (Color online) Experimental setup. Qubits ($|\psi\rangle_{A/B}$) from node A/B (shown in the lower left inset marked "Node A/B") are sent to the measurement station to perform the BSM. The time-bin single-photon qubits are prepared by modulating a stable continuous-wave (CW) laser using an intensity modulator (IM) followed by a phase modulator (PM). The electronic signals for driving the modulators are generated by an arbitrary waveform generator (AWG) and have a repetition rate of 5 MHz. The full width at half maximum (FWHM) of the pulse duration and the separation of the two temporal modes are 40 and 400 ps, respectively. The output dual-pulse train from the modulators is then attenuated to a single-photon level using a variable optical attenuator (VOA). The measurement station contains a 50/50 polarization-maintained beam splitter (50/50 PMBS) followed by two SNSPDs. The polarization controller (PC), polarization beam splitter (PBS), and FS are employed to maintain the indistinguishability of the photons upon arrival at the measurement station. The illustration on the lower right inset marked "FS" shows that the FS is realized by a PM driven by a ramp generator (RG) synchronized with the qubits. The trigger signal comes from the same AWG. To compensate the delay caused by the FS, an optical variable delay line (OVDL) with a maximum delay of 560 ps is inserted for node A. The illustration on the lower right inset marked "QST" shows that the path time delay of the unbalanced Mach-Zehnder interferometer (UMZI) used for quantum state tomography measurement matches the interval between the two temporal modes of the time-bin qubits.

(see Appendix A). Subsequently, the frequency-shifted qubits are sent to the local measurement station to perform the BSM using a 50/50 polarization-maintained beam splitter (50/50 PMBS) followed with two superconductor nanowire single photon detectors (SNSPDs). A variable optical delay line (VODL) for node A is employed to match the arrival time of qubits $|\psi\rangle_A$ and $|\psi\rangle_B$. Two polarization controllers combined with polarization beam splitters (PBSs) are utilized to align polarizations of the input photons from nodes A and B, respectively. The qubits before and after the frequency shift are measured using quantum state tomography (QST) with the same unbalanced Mach-Zehnder interferometer (UMZI) (see the lower right inset of Figure 2 marked "QST").

We first characterize the time-bin qubits $|\psi\rangle_B$ before and after the frequency-shifting using QST [26,27]. The qubit $|\psi\rangle_B$ is encoded in the states of $|e\rangle$, $|l\rangle$, and $|\pm\rangle = (|e\rangle \pm |l\rangle)/\sqrt{2}$, forming two mutually unbiased bases, i.e., the Z-basis ($|e\rangle$ and $|l\rangle$) and the X-basis ($|\pm\rangle$). The qubit with a central frequency of $f_B =$ 193.414 THz is sent to the FS for frequency shifting at three magnitudes of fs = 0 GHz (the FS is turned off), 11 GHz, and 16 GHz. Figure 3 shows the reconstructed density matrices of the quantum states of $|e\rangle$ and $|+\rangle$ (see Appendix B for more details as well as results for the quantum states of $|l\rangle$ and $|-\rangle$). We calculated the fidelities of those quantum states after the frequency-shifting by comparing them with the non-frequency-shifted (i.e., fs = 0 GHz) case. At fs = 11 GHz, the fidelities are 99.96%±0.01% for the state $|e\rangle$ and 22.53%±0.20% for $|+\rangle$, while at fs = 16 GHz, the fidelities are 99.98% and 99.60%, respectively. Although the $|e\rangle$ states maintain high fidelities (>99%), the fidelity of $|+\rangle$ state is far away from unity for the case of fs = 11.0 GHz, during the quantum state evolution caused by FS. When the time-bin qubits pass through the FS based on the phase modulator, the time-varying phase response will result in an additional phase difference $\Delta\varphi$ between the earlier and the later temporal modes. The magnitude of frequency-shifting (fs) for the time-bin qubits thus comes along with a rotation of an angle $\Delta\varphi$ in the equatorial plane, as shown in Figure 3(d). For fs = 16 GHz, the additional phase difference is close to 0 (2π) and the evolved qubit returns to its original position. For fs = 11 GHz, the evolved qubit cannot return back to the pre-position on the Bloch sphere, which will introduce bit errors in the time-bin qubit decoding (as detailed in Appendix C).

Next, we measure the indistinguishability between the time-bin qubits $|\psi\rangle_A$ and $|\psi\rangle_B$ by performing the Hong-Ou-Mandel (HOM) interference. As shown in Figure 2, two time-bin qubits $|\psi\rangle_{A/B}$ are simultaneously prepared by an AWG with identical electrical signals, where the frequencies of $|\psi\rangle_A$ and $|\psi\rangle_B$ are set to f_A = 193.414 THz and f_B. We adjust the time delay between the qubits with 10 ps accuracy and perform HOM interference with $|\psi\rangle_B$ undergoing frequency shifts of fs = 0 GHz (the FS is turned off), 11.0 GHz, and 16.0 GHz, respectively. Figure 4(a) shows the results of HOM interference with both time-bin qubits in states $|e\rangle$. When the frequency difference ($\Delta f = f_A - f_B$) between qubits

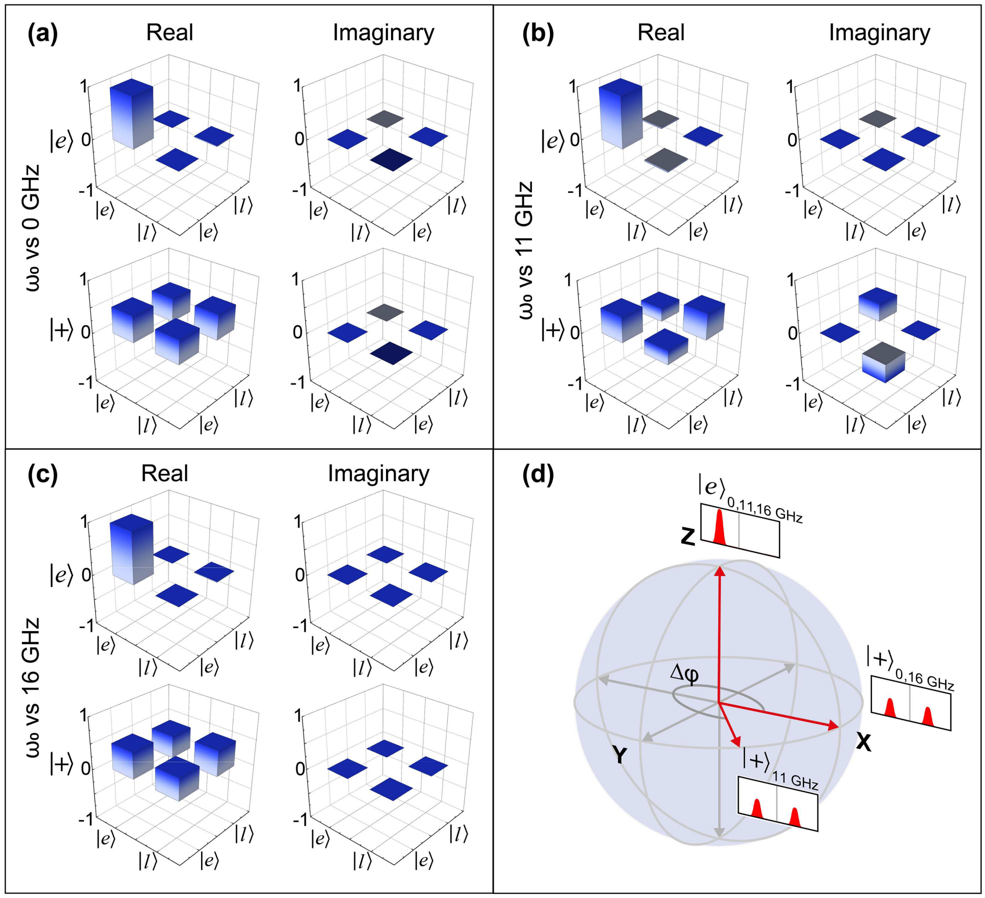

Figure 3 (Color online) Results of the density matrices. (a), (b) and (c) are the reconstructed density matrices of qubits from node B with a frequency shift of 0, 11, and 16 GHz, respectively. The central frequency of time-bin qubits $|\psi\rangle_{\mathrm{B}}$ is set to 193.414 THz. (d) Quantum state evolution of time-bin qubits on the Bloch sphere.

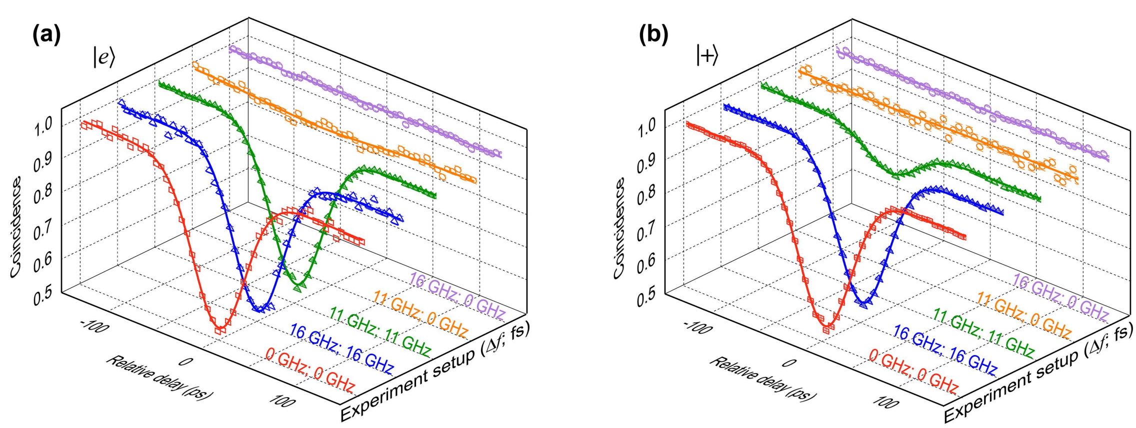

Figure 4 (Color online) HOM interference experiment results. (a) and (b) are results of HOM interference measurement between qubits of $|e\rangle$ and $|+\rangle$, respectively. In the notation (Δf; fs), Δf represents the frequency difference between time-bin qubits $|\psi\rangle_{\mathrm{A}}$ and $|\psi\rangle_{\mathrm{B}}$, and fs represents the frequency shift. In (a) ((b)), the visibilities of the red, blue, green, yellow, and purple curves are 47.37%±0.03% (45.08%±0.05%), 45.63%±0.03% (43.41%±0.06%), 45.07%±0.05% (10.69%±0.11%), close to 0, and close to 0, respectively. Experimental points are fitted with Gaussian functions. All error bars are calculated by Monte Carlo simulation assuming Poissonian detection statistics.

is set to 11 GHz (16 GHz) and FS is off, the HOM dip disappeared as shown by the yellow (purple) curve, indicating that the two qubits are distinguishable in terms of frequency. When Δf is set to match the frequency shift, (Δf = fs = 11 GHz and 16 GHz, respectively, corresponding to the green and blue curves) clear HOM dips are observed, with visibilities both exceed 45%, nearly reaching the visibility at

Table 1 Fidelities (%) of BSMs. $F_{(e/l)}$, $F_{(+/-)}$ represent the average fidelities of BSM. Test qubits are encoded as weak coherent states with an average number of photons μ, and the lower bounds of fidelities for BSM are derived for qubits encoded into single-photon states ($n = 1$) using decoy state analysis. One standard deviation uncertainties are calculated from the statistical uncertainties of photon counts.

Mean photon number	0 GHz; 0 GHz		16 GHz; 16 GHz		11 GHz; 11 GHz	
	$F_{e/l}$	$F_{+/-}$	$F_{e/l}$	$F_{+/-}$	$F_{e/l}$	$F_{+/-}$
$\mu_s = 0.0703$	98.17±0.03	72.23±0.06	97.87±0.03	76.62±0.06	98.26±0.04	33.10±0.08
$\mu_d = 0.0070$	99.37±0.12	72.18±0.47	98.54±0.22	73.47±0.52	98.80±0.29	32.60±0.68
$n = 1$	99.52±0.16	97.40±1.39	99.17±0.27	95.13±1.65	99.05±0.35	50.00±0.00

the same frequency setting of $|\psi\rangle_\mathrm{A}$ and $|\psi\rangle_\mathrm{B}$ (red curves for Δf = fs = 0 GHz, 47.37%±0.03% in our setup) without subtracting any noise counts. This result clearly indicates that the FS could effectively eliminate the frequency distinguishability between qubits with a single temporal mode (both for the cases of $|e\rangle$ and $|l\rangle$). We then perform the HOM interference with time-bin qubits $|\psi\rangle_\mathrm{A}$ and $|\psi\rangle_\mathrm{B}$ both encoded onto states $|+\rangle$, as shown in Figure 4(b). At Δf = fs = 16 GHz, the HOM interference visibility is 43.41%±0.06% as shown by the blue curve, close to the unshifted case (red curves, 45.08%±0.05% in our setup). This means that if the phase shift brings $|\psi\rangle_\mathrm{B}$ back to its original position on the Bloch sphere, the indistinguishability of the time-bin qubits could be preserved. However, in the case of Δf = fs = 11 GHz, the HOM dip decreases to 10.69%±0.11%, which is attributed to the decoherence caused by the additional phase introduced by the FS.

Finally, we performed the BSMs on different spectral channels incorporating the decoy state analysis [28], with the FS activated to eliminate frequency distinguishability. We prepared time-bin qubits with all combinations of $|\psi\rangle_\mathrm{A/B} \in [|e\rangle, |l\rangle]$ and $|\psi\rangle_\mathrm{A/B} \in [|+\rangle, |-\rangle]$. For each of the combinations of qubits, we measure nine combinations among three intensities (signal, decoy, and vacuum intensity). The mean photon numbers per qubit of the signal intensity and decoy intensity are $\mu_s = 0.0703$ and $\mu_d = 0.0070$, respectively. We record the coincidence events corresponding to projection onto one of the four Bell states $|\psi^-\rangle$. In particular, one detector clicks in the early time bin and the other detector clicks in the late time bin or vice versa [29]. The results are shown in Table 1. The fidelity of the BSM listed in Table 1 refers to the measurement discrimination fidelity, which denotes the percentage of all correct labels within the subset of all unambiguous results (as detailed in Appendix D) [30]. The fidelities $F_{e/l}$, $F_{+/-}$ are averaged over the measurement result of each set of basis vectors (e.g., $F_{e/l} = \frac{1}{2}(F_e+F_l)$) for the mean photon numbers of μ_s and μ_d, respectively. In addition, Table 1 shows the lower bounds on the fidelity that we would obtain if we performed our experiments with qubits encoded into individual photons (labelled as $n = 1$ in Table 1) without making any other changes. These bounds, denoted by $n = 1$, are derived using the decoy state analysis that underpins the security of quantum key distribution based on attenuated laser pulses (see Appendix D for further details of this method). For the qubits with a single temporal mode ($|\psi\rangle_\mathrm{A/B} \in [|e\rangle, |l\rangle]$), the fidelity $F_{e/l}$ exceeds 99% after frequency shift. For the qubits with two temporal modes ($|\psi\rangle_\mathrm{A/B} \in [|+\rangle, |-\rangle]$), the fidelity $F_{+/-}$ exceeds 0.95 when the qubit returns to the initial position on the Bloch sphere after frequency shifting (i.e., for the cases of Δf = fs = 0 GHz, 16 GHz). Otherwise, for the case of Δf = fs = 11 GHz, the fidelity decreases to $F_{+/-} = 0.50$. Therefore, the phase compensation should be taken into account when the FS is applied to the quantum systems with photons containing multiple temporal modes. Our results indicate that the single-photon FS could enable the successful connection between spectrally multiplexed elementary links. Besides the connection of spectrally multiplexed quantum elementary links, our work on spectrally multiplexed BSM can also be applied to spectrally multiplexed quantum information systems, such as MDI-QKD (see Appendix E for details).

3 Discussion and conclusion

In this paper, we propose a scheme for connecting spectrally multiplexed quantum elementary links using frequency shifting and demonstrate a proof-of-principle experiment for enabling the interconnection between adjacent elementary links with different frequencies. By using a PM driven by a ramp signal, we demonstrate frequency shifting of time-bin qubits at the single-photon level with near unity efficiency. After erasing the distinguishability of photonic qubits in the spectral domain, a projection fidelity of BSM reaches >95% between different spectral channels with decoy-state analysis. Our results show the great application potential in building long-distance quantum networks.

In our demonstration, we use a circuit to generate the ramp voltage signal. Though the ramp voltage signal has realized a near unity frequency shifting efficiency, the imperfect frequency response of electronic devices results in the slight difference in both the HOM visibilities and the BSM fidelities between the cases of non-frequency-shifting and 16 GHz frequency shifting. Meanwhile, the quantum state evolution caused by phase modulation should be taken into account, especially when the qubit is encoded onto time bins. In previous studies, photons with coherence times significantly longer than the RF modulation period have been utilized for the spectrum manipulation of time-bin qubits using PMs [31]. In contrast, our FS is designed to ensure that the entire duration of time-bin qubits is shorter than the ramp signal. This condition defines the temporal aperture of the frequency shifting [32], which thus guarantees that only linear phase modulation is applied to the qubits as well as minimizing the generation of noise photons at the operation wavelength.

Our proposed spectrally multiplexed BSM with frequency shifting shows potential for scalability if a larger frequency shift is applied. Recently developed integrated lithium niobate PMs with low π-voltage ($V_\pi = 1.4$ V, or 2.3 V for our setup) and ultra-low loss of 0.5 dB [33,34] can achieve a maximum frequency shift of 119.2 GHz through cascading. This enables access to more spectral channels and improves the efficiency of spectrally multiplexed quantum repeaters. Another approach to increase the magnitude of the frequency shift is to utilize a faster ramp generator (RG) with a higher slew-rate [35]. In the current spectrally multiplexed architecture, the frequency shift can reach $\Delta f \approx 40$ GHz with the slew-rate of 157 V/ns. The GaN-based high-voltage capacitive coupled gate driver can make the slew-rate exceeding 1000 V/ns [36], which will give the FS over a six-fold improvement. When the state-of-the-art FS is integrated into node A/B, the selectable frequency channel range can extend to more than 400 GHz. This capability enables effective utilization of the bandwidth available in multimode quantum memory (e.g., 180 GHz in [37]) and enhances the efficiency of successful entanglement swapping in quantum repeaters. Furthermore, the spectral multiplexing connection scheme based on frequency shifting does not affect its compatibility with multiplexing using other degrees of freedom. Note that for other multiplexing degrees of freedom, they can be manipulated to keep the indistinguishability of the photons. It is also worth noting that the spectral steering scheme in our system is applicable to spectral multiplexing in recent demonstrations of frequency-bin-encoded quantum key distribution [38, 39], quantum radio-frequency-over-light communication [40,41], quantum teleportation [27,42–44], and quantum secret sharing [45,46] for spectral multiplexing.

In summary, we have demonstrated connection spectrally multiplexed quantum elementary links via BSM. By defining the frequency shifting temporal aperture with a ramp voltage, we design and implement frequency shifting of the photonic time-bin. Each elementary link has spectral channels with a channel spacing of 16 GHz, and the feasibility of frequency shifting is characterized by QST, HOM interference, and BSM. Using two time-bin qubit generators within different spectral channels, a fidelity >95% is achieved for BSM projection between spectrally multiplexed elementary links. Our results thus pave the way for a future spectrally multiplexed quantum network.

Acknowledgements This work was supported by Sichuan Science and Technology Program (Grant No. 2023YFSY0061), National Natural Science Foundation of China (Grant Nos. 62475039, 62405046), Innovation Program for Quantum Science and Technology (Grant No. 2021ZD0301702), and Tianfu Jiangxi Laboratory (Grant No. TFJX-ZD-2024-002).

Supporting information Appendixes A–E. The supporting information is available online at info.scichina.com and link.springer.com. The supporting materials are published as submitted, without typesetting or editing. The responsibility for scientific accuracy and content remains entirely with the authors.

References

1 Sangouard N, Simon C, de Riedmatten H, et al. Quantum repeaters based on atomic ensembles and linear optics. Rev Mod Phys, 2011, 83: 33–80
2 Pirandola S, Laurenza R, Ottaviani C, et al. Fundamental limits of repeaterless quantum communications. Nat Commun, 2017, 8: 15043
3 Simon C. Towards a global quantum network. Nat Photon, 2017, 11: 678–680
4 Briegel H J, Dür W, Cirac J I, et al. Quantum repeaters: the role of imperfect local operations in quantum communication. Phys Rev Lett, 1998, 81: 5932–5935
5 van Loock P, Ladd T D, Sanaka K, et al. Hybrid quantum repeater using bright coherent light. Phys Rev Lett, 2006, 96: 240501
6 Simon C, de Riedmatten H, Afzelius M, et al. Quantum repeaters with photon pair sources and multimode memories. Phys Rev Lett, 2007, 98: 190503
7 Kimble H J. The quantum Internet. Nature, 2008, 453: 1023–1030
8 Vollbrecht K G H, Muschik C A, Cirac J I. Entanglement distillation by dissipation and continuous quantum repeaters. Phys Rev Lett, 2011, 107: 120502
9 Azuma K, Tamaki K, Lo H K. All-photonic quantum repeaters. Nat Commun, 2015, 6: 6787

10 Wehner S, Elkouss D, Hanson R. Quantum internet: a vision for the road ahead. Science, 2018, 362: eaam9288
11 Liu X, Hu J, Li Z F, et al. Heralded entanglement distribution between two absorptive quantum memories. Nature, 2021, 594: 41–45
12 Shchukin E, van Loock P. Optimal entanglement swapping in quantum repeaters. Phys Rev Lett, 2022, 128: 150502
13 Collins O A, Jenkins S D, Kuzmich A, et al. Multiplexed memory-insensitive quantum repeaters. Phys Rev Lett, 2007, 98: 060502
14 Zhou Z W. A multiplexed quantum repeater based on absorptive quantum memories. Sci China Inf Sci, 2021, 64: 217501
15 Lim H C, Yoshizawa A, Tsuchida H, et al. Wavelength-multiplexed distribution of highly entangled photon-pairs over optical fiber. Opt Express, 2008, 16: 22099–22104
16 Wengerowsky S, Joshi S K, Steinlechner F, et al. An entanglement-based wavelength-multiplexed quantum communication network. Nature, 2018, 564: 225–228
17 Pseiner J, Achatz L, Bulla L, et al. Experimental wavelength-multiplexed entanglement-based quantum cryptography. Quantum Sci Technol, 2021, 6: 035013
18 Donohue J M, Lavoie J, Resch K J. Ultrafast time-division demultiplexing of polarization-entangled photons. Phys Rev Lett, 2014, 113: 163602
19 Fang W T, Li Y H, Zhou Z Y, et al. On-chip generation of time-and wavelength-division multiplexed multiple time-bin entanglement. Opt Express, 2018, 26: 12912–12921
20 Gupta P, Horrom T, Anderson B E, et al. Multi-channel entanglement distribution using spatial multiplexing from four-wave mixing in atomic vapor. J Modern Opt, 2016, 63: 185–189
21 Ortega E A, Dovzhik K, Fuenzalida J, et al. Experimental space-division multiplexed polarization-entanglement distribution through 12 paths of a multicore fiber. PRX Quantum, 2021, 2: 040356
22 Sinclair N, Saglamyurek E, Mallahzadeh H, et al. Spectral multiplexing for scalable quantum photonics using an atomic frequency comb quantum memory and feed-forward control. Phys Rev Lett, 2014, 113: 053603
23 Puigibert M G, Aguilar G H, Zhou Q, et al. Heralded single photons based on spectral multiplexing and feed-forward control. Phys Rev Lett, 2017, 119: 083601
24 Ichihara M, Yoshida D, Hong F L, et al. Frequency-multiplexed Hong-Ou-Mandel interference. Phys Rev A, 2023, 107: 032608
25 Pietx-Casas O, do Amaral G C, Chakraborty T, et al. Spectrally multiplexed Hong-Ou-Mandel interference with weak coherent states. Appl Opt, 2023, 62: 3284–3288
26 Altepeter J B, Jeffrey E R, Kwiat P G. Photonic state tomography. Adv Atomic Molecular Optical Phys, 2005, 52: 105 159
27 Shen S, Yuan C, Zhang Z, et al. Hertz-rate metropolitan quantum teleportation. Light Sci Appl, 2023, 12: 115
28 Valivarthi R, Puigibert M G, Zhou Q, et al. Quantum teleportation across a metropolitan fibre network. Nat Photon, 2016, 10: 676–680
29 Rubenok A, Slater J A, Chan P, et al. Real-world two-photon interference and proof-of-principle quantum key distribution immune to detector attacks. Phys Rev Lett, 2013, 111: 130501
30 Bayerbach M J, D'Aurelio S E, van Loock P, et al. Bell-state measurement exceeding 50% success probability with linear optics. Sci Adv, 2023, 9: eadf4080
31 Xue R, Liu X, Li H, et al. Measurement-device-independent quantum key distribution of frequency-nondegenerate photons. Phys Rev Appl, 2022, 17: 024045
32 Wright L J, Karpiński M, Söller C, et al. Spectral shearing of quantum light pulses by electro-optic phase modulation. Phys Rev Lett, 2017, 118: 023601
33 Hu Y, Yu M, Zhu D, et al. On-chip electro-optic frequency shifters and beam splitters. Nature, 2021, 599: 587–593
34 Wang C, Zhang M, Chen X, et al. Integrated lithium niobate electro-optic modulators operating at CMOS-compatible voltages. Nature, 2018, 562: 101–104
35 Luo Y, Sun C Z, Xiong B, et al. High-speed optoelectronic devices. Sci China Inf Sci, 2023, 66: 150401
36 Moench S, Hillenbrand P, Hengel P, et al. Pulsed measurement of sub-nanosecond 1000 V/ns switching 600 V GaN HEMTs using 1.5 GHz low-impedance voltage probe and 50 Ohm scope. In: Proceedings of IEEE 5th Workshop on Wide Bandgap Power Devices and Applications (WiPDA), 2017. 132–137
37 Zhang X, Zhang B, Wei S, et al. Telecom-band-integrated multimode photonic quantum memory. Sci Adv, 2023, 9: eadf4587
38 Kashi A K, Kues M. Frequency-bin-encoded entanglement-based quantum key distribution in a reconfigurable frequency-multiplexed network. Light Sci Appl, 2025, 14: 49
39 Yan Z, Jia X. Quantum key distribution with chromatic codes. Light Sci Appl, 2025, 14: 126
40 Liang S, Cheng J, Qin J, et al. High-speed quantum radio-frequency-over-light communication. Phys Rev Lett, 2024, 132: 140802
41 Liang S, Cheng J, Qin J, et al. Frequency-division multiplexing continuous variable quantum dense coding with broadband entanglement. Laser Photon Rev, 2024, 18: 2400094
42 Yan Z, Jia X. Teleportation goes to Hertz rate. Light Sci Appl, 2023, 12: 167
43 Yan J, Zhou X, Qin Y, et al. Deterministic and multiuser quantum teleportation network of continuous-variable polarization states. Phys Rev Res, 2024, 6: L032062
44 Ren S Y, Han D M, Wang M H, et al. Continuous variable quantum teleportation and remote state preparation between two space-separated local networks. Sci China Inf Sci, 2024, 67: 142502
45 Xiao Y R, Jia Z Y, Song Y C, et al. Source-independent quantum secret sharing with entangled photon pair networks. Opt Lett, 2024, 49: 4210–4213
46 Qin Y, Cheng J, Ma J, et al. Efficient and secure quantum secret sharing for eight users. Phys Rev Res, 2024, 6: 033036